

# Cavity-enhanced superradiant Rayleigh scattering with ultra-cold and Bose-Einstein condensed atoms

Sebastian Slama, Gordon Krenz, Simone Bux, Claus Zimmermann, and Philippe W. Courteille  
*Physikalisches Institut, Eberhard-Karls-Universität Tübingen,  
 Auf der Morgenstelle 14, D-72076 Tübingen, Germany*

(Dated: August 15, 2018)

We report on the observation of collective atomic recoil lasing and superradiant Rayleigh scattering with ultracold and Bose-Einstein condensed atoms in an optical ring cavity. Both phenomena are based on instabilities evoked by the collective interaction of light with cold atomic gases. This publication clarifies the link between the two effects. The observation of superradiant behavior with thermal clouds as hot as several tens of  $\mu\text{K}$  proves that the phenomena are driven by the cooperative dynamics of the atoms, which is strongly enhanced by the presence of the ring cavity.

PACS numbers: 42.50.Gy, 03.75.-b, 42.60.Lh, 34.50.-s

## I. INTRODUCTION

The interaction of light with atomic gases takes place in most cases as a local process: Light shone into an atomic cloud is scattered by individual atoms. In principle, every atom having scattered a photon can be detected through the momentum imparted to it by photonic recoil, and in general, the scattering process is ignored by all other atoms. This holds even for Bose-Einstein condensates (BEC), which are pure quantum states consistent of an ensemble of delocalized atoms. There are however prominent exceptions: Dicke superradiance [1] is a well-known synchronization phenomenon in spontaneous emission. It is observed, for instance, as a collective deexcitation of an ensemble of inverted atoms with an accelerated rate, which scales with the square of the number of inverted atoms [2]. Another example is the collective absorption of photonic recoil by an ensemble of atoms tight together by strong forces known as Mößbauer effect [3, 4].

Collective effects in light scattering arise when the scatterers are mutually coupled by interactions or display long-range order. Often the collective coupling involves mechanical forces, for example photonic recoil or the electrostrictive force arising from dipole-dipole interactions. In both cases, the interatomic force originates from a radiative interaction, or using fully quantized terms, the transfer of phonons is mediated by an exchange of photons. Compared to short-ranged binary collisions radiation-based interaction extends much further in space. Under some circumstances it can be completely delocalized. In some cases, collective coupling can trigger instabilities. Well-known examples for instabilities in the field of nonlinear optics are stimulated Raman scattering, stimulated Brillouin scattering or the collective atomic recoil laser (CARL) [5, 6, 7, 8, 9].

Collective instabilities have recently been observed in clouds of cold and ultra-cold atoms driven by light [7, 10, 11, 12, 13, 14, 15]. In the present paper, we focus on two types of experiments, dealing with the superradiant Rayleigh scattering (SRyS) phenomenon on one hand [10,

11, 12] and the collective atomic recoil laser [7] on the other.

CARL is observed, when a strong pump field is shone onto an atomic gas. This leads to the exponential growth of an unpumped probe light field and to the formation of an atomic density grating [5, 6]. If pump and probe light field are counter-propagating modes of a high-finesse ring cavity, the interaction time of the light fields with the atoms can be enhanced by several orders of magnitude, which supports the amplification. Consequently, all CARL experiments carried out up to date employed ring cavities [7, 8, 9]. Therefore, in this paper we will use the term CARL in the tight sense of a cavity-assisted collective instability, although the CARL has originally been postulated without cavity [5].

SRyS has first been observed in Bose-Einstein condensed atomic clouds. A short laser pulse shone onto the cloud is scattered from atoms of the BEC, which then by photonic recoil form motional sidemodes. Matter-wave interference between the recoiling atoms and the BEC at rest leads to the formation of an atomic density grating thereby exponentially enhancing the scattering. SRyS was originally attributed to four-wave mixing between optical and matter waves, bosonically stimulated by the macroscopic occupation of the final momentum state. Already in the pioneering work [10] it was recognized that SRyS does not require quantum degeneracy and would in principle also work in a thermal cloud. Nevertheless the terminology of bosonic stimulation and the fact that SRyS could at first not be observed with thermal clouds led to some obscurity and discussions about the role of quantum statistical effects. Theoretic work [16, 17] showed that the gain mechanism is independent of the quantum statistics and should in principle also be observable with fermionic and thermal atoms. The experimental prove was given by the observation of CARL [7] and SRyS with thermal gases [18]. The important feature is not the quantum state of the atoms but the cooperative behavior.

CARL has a close analogy with SRyS, since they both share the same gain mechanism [19]. However in contrast to SRyS, CARL activity has been observed with thermal

atoms as hot as a few 100  $\mu\text{K}$  [7]. This fact raises the question, what distinguishes both collective effects. In both experiments there must be a coherent mechanism correlating the individual scattering events. Coherence can be transferred between scattering events either via de Broglie waves interference or optical interference.

SRyS is difficult to observe with thermal atomic ensembles, because the coherence is stored in the momentum states of the atoms. Thermal motion of atoms therefore Doppler-limits the coherence time of the system [18]. CARL is much less sensitive to the thermal motion of the atoms, because the coherence is stored in the light field of the cavity. The density-of-states in the cavity restricts the frequency of the scattered light to values close to one of its eigenfrequencies. In the case of a so-called good-cavity this is equivalent to the fact that the atomic momentum states which can be populated by photonic momentum transfer are limited to a few low-lying states. This effect counteracts momentum diffusion which can occur due to a thermal motion of the atoms, but is also intrinsically connected with the collective gain process itself.

We organized this paper as follows: In section II we expose the problem of motion-induced collective effects in light scattering. In particular, we will discuss the intricate relationship between CARL and SRyS, pointing out the common features and the differences. We will then briefly introduce the mathematical models we use to reproduce our observations in simulations. Ideally, in a perfectly homogeneous cloud the collective instability would start from quantum fluctuations in the reverse mode, thermal excitations of this mode being completely frozen out at room temperature. However, thermal fluctuations in the atomic density distribution and, even more important, spurious light scattering at the surfaces of the cavity mirrors scatter a certain amount of light into the reverse mode, which is sufficient to seed the instability. It is thus important to incorporate mirror backscattering in realistic theoretical models, as we will show in section IID. Section III is devoted to presenting our experimental apparatus, the temporal sequence of an experimental run and several measurements. In particular, we will show the measured dependences of the collectively scattered light power on various parameters, such as atom number, pump power, and mirror backscattering. We will demonstrate that both regimes, the good- as well as the bad-cavity regime, can be realized and exhibit characteristic signatures. In section III F, we present and discuss time-of-flight absorption images taken on thermal and Bose-condensed atomic clouds. We conclude this paper with a discussion and a brief outlook.

## II. THEORETICAL BACKGROUND

CARL and SRyS have been observed under very different experimental circumstances and in different param-

eter regimes. In the case of CARL the atoms are stored in a ring cavity, for SRyS they are held in free space. CARL can be observed with 100  $\mu\text{K}$  cold atoms [7], while SRyS requires temperatures lower than 1  $\mu\text{K}$  and is hardly seen with thermal clouds. Finally, CARL is seen with pump laser detunings, which are 3 or 4 orders of magnitude larger, than for SRyS.

Nevertheless, both phenomena have an important feature in common. They share the same gain mechanism based on collective light scattering and leading to an exponential instability in the atomic density distribution and to the emission of coherent light pulses. In this section, we will summarize and combine the main theoretical results published in [10, 20, 21] in order to clarify the connection between CARL and SRyS in a consistent picture supporting the understanding of our measurements. Later we derive equations of motion valid in both regimes of CARL and SRyS.

### A. Self-amplification in CARL and SRyS

In the CARL experiments [7, 8, 9], a cold or ultracold atomic cloud is brought into the mode volume of a unidirectionally pumped ring cavity. The pump light is very far detuned by more than 1 nm. It is irrelevant whether the cloud is condensed or thermal. The atoms scatter light from the pumped into the reverse mode. Tiny fluctuations in the nearly homogeneous atomic density distribution are exponentially amplified. The atoms self-organize into a one-dimensional optical lattice and a red-detuned coherent probe light is emitted by the reverse mode.

The Rabi frequency generated by a single photon in the ring cavity of round-trip length  $L$  and waist  $w_0$  is  $\Omega_1 = \sqrt{3\Gamma c/k^2 w_0^2 L}$  [22, 23]. The single-photon light-shift far from resonance,  $U_0 = \Omega_1^2/\Delta$ , can also be interpreted as the Rabi frequency for the coupling between the pump and the probe mode, i.e. the rate at which photons are exchanged between the modes. The small signal gain can be derived from a linearization of the CARL equations [20, 21],

$$G_c = \frac{2g^2 N}{\kappa_c}, \quad (1)$$

where  $N$  is the atom number and  $\kappa_c = \pi\delta_{\text{fsr}}/F$  the decay rate of the light field in the cavity.  $\delta_{\text{fsr}}$  is the free spectral range of the cavity and  $F$  its finesse. The quantity  $g$  is given by

$$g = \frac{\Omega_+ \Omega_-}{2\Delta}, \quad (2)$$

where the Rabi frequency generated by the pump mode scales with the root of the pump photon numbers,  $\Omega_+ = \Omega_1 \sqrt{n_+}$ . The coupling strength in the probe mode is

$\Omega_- = \Omega_+$ . From the above equations, we get

$$G_c = \frac{\Omega_+^2 N \Omega_-^2}{2\Delta \kappa_c \Delta}. \quad (3)$$

In the SRyS experiments performed up to date [10, 11, 12, 18, 24], an ultracold, in general Bose-condensed atomic cloud with ellipsoidal shape is irradiated by a short pump laser pulse modestly detuned from an atomic resonance by about 1 GHz. The pulsed pump light drives a transient dynamics simultaneously forming a matter wave grating and emitting an optical mode into the BEC's long axis, which exponentially amplify each other.

Following Ref. [10], one may associate the part of the BEC that corresponds to atoms which have scattered a photon with an atom number  $N_r$ . The remaining part consists of  $N$  atoms. The density is modulated by interference between the two parts of the wave function, and the number of atoms that form the density modulation is  $N_{\text{mod}} \propto \sqrt{2NN_r}$ . As for usual Bragg scattering or Dicke superradiance the number of photons  $n$  scattered at the density modulation is  $n \propto N_{\text{mod}}^2 \propto N_r$ . Since every scattered photon generates a recoiling atom, the number of recoiling atoms increases like  $\dot{N}_r \propto n$ , and we get  $\dot{N}_r = G_{\text{sr}} N_r$ , i.e. an exponential increase of recoiling atoms with a gain factor  $G_{\text{sr}}$ . This increase is mirrored by an identical rise of the number of scattered photons, which results in a gain mechanism for the scattered light mode. The incident and the scattered light mode are coherently coupled, just like in the case of CARL, so that in principle the scattered photons can be scattered back into the incident mode.

The superradiant gain can be expressed as

$$G_{\text{sr}} = RN_0 \frac{\Phi_s}{8\pi/3}, \quad (4)$$

where  $R = \Gamma\Omega_+^2/(4\Delta^2 + 2\Omega_+^2 + \Gamma^2)$  is the single-atom Rayleigh scattering rate, with  $\Gamma$  being the linewidth of the atomic resonance,  $\Delta$  the detuning, and  $\Omega_+$  the Rabi frequency generated by the incident laser beam.  $\Phi_s \simeq \lambda^2/\pi w^2$  is the scattering solid angle, with  $w$  being the waist of the condensate. Hence, far from resonance,

$$G_{\text{sr}} = \frac{\Omega_+^2}{\Delta^2} N_0 \frac{3\Gamma}{2k^2 w^2}. \quad (5)$$

This result can be brought into the same form as the CARL gain (3), if we interpret the condensate, whose length along the long axis is  $L$ , as a cavity with free spectral range  $\delta_{\text{fsr}} = c/L$  and finesse  $F_{\text{sr}} = \pi$ . With this interpretation the decay rate of the light mode scattered by the condensate is given by the residence time of the light within the BEC [25],  $\kappa_{\text{fsr}} = \pi\delta_{\text{fsr}}/F_{\text{sr}} = c/L$ .

$$G_{\text{sr}} = \frac{\Omega_+^2}{2\Delta^2} \frac{N_0}{\kappa_{\text{sr}}} \frac{3\Gamma\delta_{\text{fsr}}}{k^2 w^2} = \frac{\Omega_+^2}{2\Delta} \frac{N_0}{\kappa_{\text{sr}}} \frac{\Omega_1^2}{\Delta}. \quad (6)$$

This result shows the equivalence of the superradiant gain and the gain occurring in CARL in equation (3).

The formal identity of the small signal gain of CARL and SRyS points to the same roots of both phenomena. Nevertheless, their respective experimental circumstances are quite different. The differences become most apparent in the simultaneous build-up of the atomic density grating and optical standing wave, occurring as well in CARL as in SRyS. The difference lies in the storage of the coherence, which is crucial in order to sustain the build-up process. In principle the coherence can either be stored as a matter wave coherence between different atomic momentum states or as a phase coherence between the two involved light fields. In SRyS the optical coherence time alone would be very small, as can be estimated from the decay rates of the optical modes, which are on the order of  $\kappa_{\text{sr}} \simeq 10^{12} \text{ s}^{-1}$ . The coherence must therefore be maintained in the atomic momentum states which then form a matter wave grating. This is the reason why SRyS is very sensitive to the temperature of the atomic cloud. The thermal energy of the atoms must be smaller than the recoil energy  $k_B T < \hbar\omega_r = 2\hbar^2 k^2/m$ . Otherwise, the Doppler broadening leads to decoherence of the momentum states and destroys the matter wave coherence and the resulting density grating.

For CARL the situation is reversed. CARL has been observed with temperatures much higher than the recoil temperature, i.e. in a regime where interferences between atoms in Raman superpositions of momentum states are quickly smeared out by Doppler broadening. Here, the optical cavity plays the crucial role, because it phase-coherently stores the participating light fields for times on the order of several  $\mu\text{s}$ , given by the cavity decay rate  $\kappa_c/2\pi = 20 \text{ kHz} \ll \kappa_{\text{sr}}$  which is 7 orders of magnitude smaller than in the case of SRyS without cavity.

## B. Collective gain in various regimes

The important point is now, that the broad range in which the collective gain can be varied in our experiment allows us to study CARL and SRyS dynamics as two opposite regimes of one system, called the good-cavity and the bad-cavity regime. Both regimes can be further divided into a semiclassical and a quantum domain and are characterized by two parameters, the CARL parameter  $\rho$  and the scaled decay rate  $\kappa$  [19]. The CARL parameter is given by the product of the small signal gain and the decay rate of light both in units of the recoil frequency  $\omega_r = 2\hbar k^2/m$

$$\rho^3 = \frac{G_{\text{c,sr}}}{\omega_r} \cdot \frac{\kappa_{\text{c,sr}}}{\omega_r}. \quad (7)$$

The scaled decay rate  $\kappa = \kappa_{\text{c,sr}}/\omega_r \rho$  depends via  $\rho$  on the gain, too. The good-cavity regime is given by  $\kappa < 1$ , the bad-cavity regime by  $\kappa > 1$ .

For the interpretation it is helpful to link the gain  $G_{c,SR}$  to the gain bandwidth  $\Delta\omega_G$ , which is defined as the width of spectral range where the light scattering is exponentially amplified [19]. Let us first consider the semiclassical regime. The good-cavity limit is reached for strong saturation of the transition between the coupled cavity modes. This means that the gain, which can be interpreted as Rabi frequency, overwhelms the cavity decay width,  $G_{c,SR} \gg \kappa_{c,SR}$ . In this regime the transition is power-broadened by an amount  $\Delta\omega_G \sim \omega_r \rho$  (see Fig. 1). This refers to the CARL experiments performed so far, where the gain bandwidth is proportional to the CARL parameter. In contrast, the bad-cavity regime is reached for small gain,  $G_{c,SR} \ll \kappa_{c,SR}$ . In this case, the gain bandwidth is given by the cavity decay rate,  $\Delta\omega_G \sim \kappa_{c,SR}$ . Obviously, the resolution of the gain profile cannot be better than  $\kappa_{c,SR}$ . This is the typical situation of SRyS.

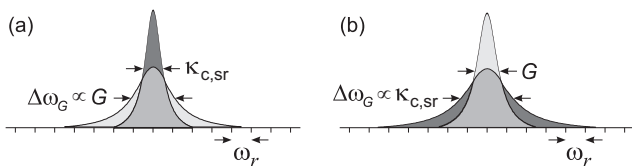


FIG. 1: Representation of the two limiting cases of a long and short cavity lifetime. Shown are the cavity transmission profile (dark shaded areas) and the gain profile (bright shaded areas). (a) When the cavity linewidth is smaller than the gain, the good-cavity limit is realized. (b) When the gain is smaller, the superradiant limit is realized.

The distinction between semiclassical and quantum regime is based on the characteristic scale set by the recoil frequency  $\omega_r$ . In the semiclassical regime the gain bandwidth is large enough to amplify many adjacent momentum states of the quantized motion  $\Delta\omega_G > \omega_r$ , whereas in the quantum regime only one momentum state can be amplified at a time  $\Delta\omega_G < \omega_r$ . Both, the semiclassical as well as the quantum regime have been studied in Ref. [24] in the bad-cavity limit by varying the gain bandwidth. Strictly the CARL gain (1)-(3) is only valid in the quantum regime. In this regime the equivalence to the SRyS gain (4)-(6) appears in its clearest way. In the semiclassical regime valid for our experiment the CARL gain is reduced [21], as has also been observed in SRyS [24]. In our experiment, the quantum limit could be reached by reducing atom number and pump power. This would however generate signals which are below the detection limit of our current setup. Nevertheless, small deviations due to the quantum nature of the atomic motion are expected, as will be briefly discussed in the next sections.

### C. Equations of motion for atoms in a ring cavity

The system under consideration consists of ultra-cold or Bose-condensed atoms interacting with two counter-propagating modes of an optical cavity. The most general

approach would treat all modes as quantized, in particular the atomic cloud would be described by a second-quantized matter wave field [26, 27]. Such an approach is necessary whenever mean field interactions or quantum statistical effects, like non-local interparticle correlations, particle fluctuations or entanglement, play a role. In the circumstances of our experiments, however, several simplifications can be made.

1. All electronically excited states may be adiabatically eliminated [6, 22]. The detuning of the pump laser beam from the nearest resonance frequencies of the rubidium atom is so large, that the internal dynamics is continuously at a steady state keeping the population of the excited states at a negligible level.
2. Propagation effects of light inside the atomic cloud [28, 29] do not need to be considered. In comparison with the SRyS experiments, where the pump light is generally detuned by amounts on the order of 1 GHz, our experiment uses 1000 times larger detunings. Hence, the optical density of our atomic clouds at these detunings is negligibly small.
3. Quantum statistical effects, such as entanglement, are predicted to occur naturally as a result of CARL dynamics [27]. However, our experiment is not sensitive to signatures arising from quantum statistics.
4. We treat all light fields classically. The mode volume of our cavity is of a size that the atom-field coupling constant larger than the cavity decay width, but it is much smaller than the spontaneous emission decay width of the atomic transition. Hence we are far from the cavity QED regime. Even in situations where shot noise could play a role, e.g. in seeding the instability, perturbations arising from experimental imperfections (mirror backscattering) dominate.
5. We treat the problem in one dimension, i.e. along the optical axis of the cavity. Transversal oscillations of the atomic cloud, which may result from the collective dynamics [14] are not considered here.
6. We neglect the backaction of the atoms on the pump light field (undepleted pump approximation). This is possible because the probe light is typically three orders of magnitude weaker than the pump field. In the experiment, the pump laser is tightly phase-locked to a cavity eigenfrequency. Consequently, as pointed out in Ref. [7], we can suppose a fixed phase relation between the incident pump laser field (labeled by the electric field amplitude normalized to the field generated by a single photon),  $\alpha_{in}$ , and the pumped cavity mode,  $\alpha_+ = \alpha_{in} \sqrt{\delta_{f,SR}/\kappa_c}$ . The phase can be arbitrarily chosen, e.g.  $\alpha_+$  can be taken as real.

Even though quantum statistical effects do not emerge from our measurements at temperatures close to or below the recoil limit the quantized nature of the atoms' motion influences their dynamics, as described by a model derived by Piovella and coworkers [19]. Within this model and in the approximations specified above, the CARL

Hamiltonian for an ensemble of  $N$  atoms reads

$$H = \frac{1}{2m} \sum_{j=1}^N \hat{p}_j^2 + \hbar\Delta_c (|\alpha_-|^2 + |\alpha_+|^2) \quad (8)$$

$$+ \hbar U_0 \alpha_+ \sum_{j=1}^N (\alpha_-^* e^{-2ik\hat{z}_j} + h.c.) ,$$

where  $U_0$  is the single-photon light shift, and  $\Delta_c$  the detuning between pump and probe. The motional degrees of freedom, i.e. the position  $\hat{z}_j$  and the momentum  $\hat{p}_j$  of every atom, satisfy the following commutation relation  $[\hat{z}_j, \hat{p}_{j'}] = i\hbar\delta_{jj'}$ . From the Heisenberg equations  $i\hbar\dot{\hat{z}} = [\hat{z}, H]$  and  $i\hbar\dot{\hat{p}} = [\hat{p}, H]$  we derive the equations of motion for the coupled system,

$$\frac{d\hat{z}_j}{dt} = \frac{\hat{p}_j}{m} , \quad (9)$$

$$\frac{d\hat{p}_j}{dt} = -2i\hbar k U_0 \alpha_+ (\alpha_-^* e^{2ik\hat{z}_j} - \alpha_- e^{-2ik\hat{z}_j}) ,$$

$$\frac{d\alpha_-}{dt} = -(\kappa_c + i\Delta_c)\alpha_- - iU_0\alpha_+ \sum_{j=1}^N e^{-2ik\hat{z}_j} .$$

In the last equation cavity damping has been introduced phenomenologically.  $\hat{b} \equiv N^{-1} \sum_j e^{-2ik\hat{z}_j}$  measures the degree of atomic bunching. Starting from these equations, we either treat the motion classically or quantized [19, 30]. In the first case, we simply replace the position and momentum operators by their classical expectation values. These are the basic equations used to model most of the curves shown in this paper [31].

In order to check, whether quantum effects of the motion have an impact on the collective dynamics, we have derived from (8) a master equation for the density operator defining a momentum basis  $|n\rangle_j$  such that  $\hat{p}_j |n\rangle_j = 2\hbar kn |n\rangle_j$  and  $|\psi(\theta_j)\rangle = \sum_n c_j(n) |n\rangle_j$ . The calculations, which are analogous to those presented in Ref. [19], are not reproduced here. They basically show that, for the parameters used in our experiments, quantum effects of the atomic motion are small. I.e., using the terminology of Ref. [19], we are in the semiclassical regime.

#### D. Modeling mirror backscattering and radiation pressure

Perturbative effects resulting from backscattering from the mirror surfaces and from radiation pressure have been neglected so far. Unfortunately, we found both effects to influence the experimental observations, so that this idealization has to be given up. Let us first discuss mirror backscattering. Dust particles or irregularities on the mirror surfaces can scatter light from a cavity mode into the counterpropagating mode. This effect is well-known in laser gyroscopes, where it leads to phase-locking. Interestingly, the effect is the more pronounced the better

the reflectivity of the mirrors and hence the finesse of the cavity [23]. In principle, to describe mirror backscattering, one has to know the precise locations of the scatterers on the mirrors. As we explain in another paper [32], we can describe their influence by a single scatterer localized at position  $z_s$  with a wavelength-dependent scattering rate  $U_s$ . The scattering can be modeled in the very same way as backscattering from atoms, except for the fact that the scatterers are now fixed in space. Hence, we may just replace the Hamiltonian (8) by

$$H' = H + \hbar U_s \alpha_+ (\alpha_-^* e^{-2ikz_s} + h.c.) . \quad (10)$$

The resulting modified equations of motion are only changed by an additional term for the evolution of the field amplitude. I.e. the third of the equations (9) is supplemented with a gain rate  $iU_s\alpha_+$  for the probe mode resulting from photons scattered out of the pump mode by mirror backscattering. In the experiment, we determine the amount of mirror backscattering  $U_s$  from independent measurements.

Radiation pressure is due to spurious population of electronically excited states under the influence of the pump laser beam. Although, far from resonance the effect is weak, it still leads to a noticeable acceleration of the atoms. Gangl and Ritsch [22] have shown that the adiabatic elimination of electronically excited states introduces additional contributions in the classical CARL equations scaling with the Rayleigh scattering rate  $\gamma_0$ . This describes the effect of recoil heating due to radiation pressure

$$m \frac{d^2 z_j}{dt^2} = -\hbar k \gamma_0 (|\alpha_+|^2 - |\alpha_-|^2) \quad (11)$$

$$- 2i\hbar k U_0 \alpha_+ (\alpha_- e^{2ikz_j} - \alpha_-^* e^{-2ikz_j}) ,$$

$$\frac{d\alpha_-}{dt} = -(\kappa_c + N\gamma_0)\alpha_- - N(\gamma_0 + iU_0)\alpha_+ b - iU_s\alpha_+ .$$

The additional contributions not only lead to losses for the light mode, but also exert an accelerating force onto the atoms. Experimentally, we observe a broadening of the momentum distribution by recoil heating which slightly impairs the collective dynamics for measuring times longer than 100  $\mu$ s.

### III. MEASUREMENTS

We describe our experimental setup tracking the temporal sequence of an experimental run. The whole setup (shown in Fig. 2) consisting of magnetic coils, wires and the ring cavity is placed inside a ultra-high vacuum chamber pumped by a cryogenic titanium sublimation pump and a 20l/s ion getter pump to a pressure of about  $10^{-11}$  mbar. Heat produced in coils and wires inside the vacuum is dissipated via a temperature-stabilized cooling rod to a liquid nitrogen reservoir. A second vacuum

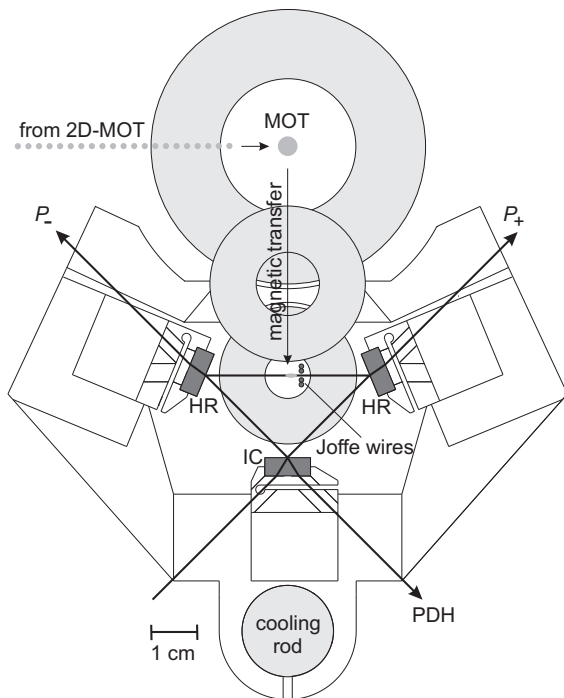


FIG. 2: Technical drawing of the setup in the main chamber including coils for magnetic and magneto-optical trapping, wires for a Joffe-Pritchard type trap and the ring cavity. All pieces are held together by massive copper parts omitted in this figure for clarity.

chamber is connected with this main chamber via a differential pumping hole and contains a Rb partial pressure of several  $10^{-7}$  mbar. The second chamber accommodates a two-dimensional magneto-optical trap (2D-MOT) producing a cold atomic beam directed into the main chamber. From this atomic beam about  $10^8$  atoms/s are recaptured in a standard magneto-optical trap (MOT) in the main chamber. After the MOT has been loaded for 15 s, the atoms are transferred into a magnetic trap produced by the same coils as the MOT. On a typical day, we load about  $2 \times 10^8$  atoms at a temperature of  $T = 100 \mu\text{K}$  into the magnetic trap. The atoms are then magnetically transferred via a second into a third pair of coils, whereby the atoms are compressed adiabatically. The magnetic quadrupole field gradient between the third pair of coils is 160 G/cm in the horizontal and 320 G/cm in the vertical direction. With two pairs of wires separated by 1 mm and running parallel to the symmetry axis of the coils a Joffe-Pritchard type potential is created [33]. Typical values of the oscillation frequencies in this trap are  $\omega_r/2\pi = 200$  Hz and  $\omega_z/2\pi = 50$  Hz at a magnetic offset field of  $B_0 = 2$  G with the  $z$ -direction pointing along the cavity mode through the gap between the wires. The vertical position of the wire trap can easily be shifted by the currents in the quadrupole coils. Inside the wire trap the atoms are cooled by forced evaporation: a microwave frequency is tuned resonantly to the ground state hyperfine structure and couples the trapped

Zeeman state  $|2, 2\rangle$  and the untrapped state  $|1, 1\rangle$ . We ramp down the frequency for 15 s starting from a detuning of 210 MHz and reach quantum degeneracy at a detuning of about 4 MHz with about  $N = 5 \times 10^5$  atoms at  $T_c = 800$  nK. Almost pure condensates of  $N = 2 \times 10^5$  atoms can be achieved by ramping down to even lower frequencies. When the evaporative cooling stage is completed, the cold atoms are vertically transferred into the mode volume of the ring cavity. The ring cavity consists of one plane (IC) and two curved (HR) mirrors with a curvature radius of  $R_c = 10$  cm. The round-trip length of the cavity is 8.5 cm, corresponding to a free spectral range of  $\delta_{\text{fsr}} = 3.5$  GHz. One of the two counterpropagating modes is continuously pumped by a titanium-sapphire laser. The laser can be stabilized to this mode using the Pound-Drever-Hall (PDH) method. The quality factor of the cavity depends on the polarization of the incoupled light. For p-polarized light, a finesse of  $F = 87000$  is determined from a measured intensity decay time of  $\tau = 3.8 \mu\text{s}$ . For s-polarized light the finesse is 6400.

### A. Experimental procedure

The measurements are performed in the following way. A cloud of cold atoms is magnetically transferred into the cavity. During this time the cavity is not pumped with light in order to prevent losses of atoms due to Rayleigh scattering. This implies that the frequency of the laser

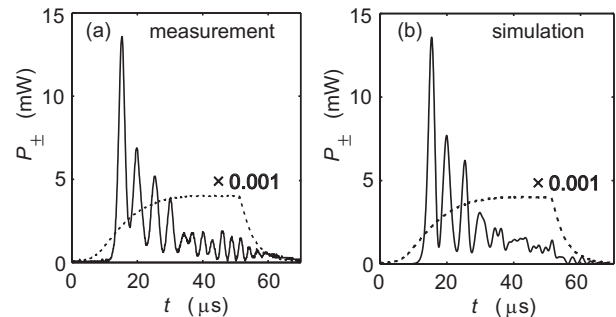


FIG. 3: (a) Typical measured time signal (solid line) of the probe-light power. Experimental parameters are  $N = 1.5 \cdot 10^6$ ,  $P_+ = 4$  W,  $\lambda = 797.3$  nm and  $F = 87000$ . For visibility the pump-light power (dashed line) is scaled down by a factor of 0.001. (b) Simulation of the CARL equations. The measured rise of the pump-light power is used in the simulation and the experimental parameters are fitted in order to agree with the measured time curve. The fitted parameters ( $P_+$ ,  $N$ ) are in reasonable agreement with the measured parameters.

cannot be stabilized to a mode of the cavity during the transfer. As soon as the atoms are inside the cavity, we switch on the pump light again and ramp its frequency across the cavity resonance. This is done by means of a piezo-electric transducer normally controlled by the slow branch of the Pound-Drever-Hall (PDH) servo, which is interrupted for this reason. As soon as the frequency

is close to the cavity resonance, the fast branch of the PDH servo acting on an acousto-optic modulator (AOM) quickly pulls the laser frequency to the center of the resonance and tightly locks its phase, thus compensating for the frequency ramp. After a time of about  $50 \mu\text{s}$  the pump light is turned off. The build-up time for the ring cavity pump mode is limited by the bandwidth of the locking servo to about  $\tau_{bw} = 20 \mu\text{s}$ , which is longer than the cavity decay time.

As soon as the pump mode power builds up in the ring cavity, the collective dynamics results in light scattering into the cavity probe mode. The limited build-up time of the pump power leads to a delayed and slightly weaker dynamics as compared to a rapid switch-on. We study this dynamics mainly via the evolution of the recorded probe light power  $P_-$ . The time signal of the probe light shows characteristic maxima and minima like the ones presented in Fig. 3. This behavior can be explained most easily in the case, where the atoms occupy a initial momentum eigenstate and are coupled by the coherent dynamics to a final momentum state. The temporal evolution is a Rabi oscillation-like change of occupation from the initial to the final state. This causes the build-up of an atomic density grating which reaches its maximum with half of the atoms in each state and zero contrast when all atoms are in the initial or the final state. The scattered light is proportional to this density grating contrast. Maxima in the probe light power therefore occur with each change of the momentum state. In the situation depicted in Fig. 3 the dynamics leads to the simultaneous occupation of an increasing number of momentum states. The maximum atomic density grating washes out with time and we observe a decrease of the light power maxima.

In the following we analyze the probe light power reached at the first maximum  $P_{-,1}$ , because it shows a clear dependence on atom number  $N$ , pump light power  $P_+$ , laser wavelength  $\lambda$ , finesse of the cavity  $F$ , and on the atomic cloud's temperature  $T$ . In contrast, it is quite robust against perturbative effects such as mirror backscattering. Simulations of the CARL dynamics like shown in Fig. 3(b) are performed by numeric integration of (11) with the explicit Euler method. We simulate the trajectories of  $N_s = 100$  atoms, each representing  $N/N_s$  real atoms. At the beginning of the simulation the atoms are spread in position over half a wavelength with equal spacings. For simulations of clouds with temperature  $T = 0$  the start momentum of all atoms is set to  $p_j = 0$ . For simulations of clouds with nonzero temperature the momenta at the beginning are normally distributed with  $\langle p_j^2 \rangle = mk_B T$ .

## B. Mirror backscattering

Scattering from the mirror surfaces leads to the presence of light in the probe mode even in the absence of atoms in the cavity. In the presence of atoms, this

light influences the atomic collective dynamics. Fig. 4 shows the impact of mirror backscattering on the height of the first maximum  $P_{-,1}$  and on the time delay  $\Delta t$  from switching on the pump until the maximum is reached.

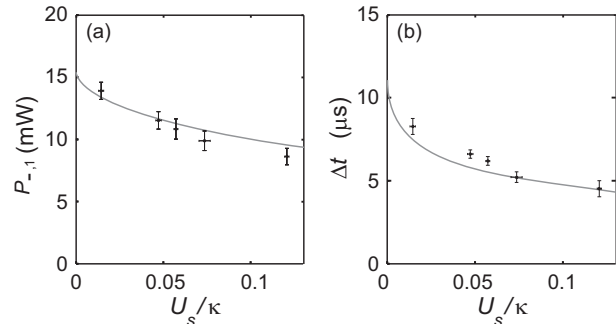


FIG. 4: Influence of mirror backscattering (a) on the peak probe power  $P_{-,1}$  and (b) on the delay of this peak  $\Delta t$ . The rate of mirror backscattering  $U_s$  is given in units of the cavity decay rate  $\kappa$ . Measurements (circles) and simulations (lines) show a decrease of both  $P_{-,1}$  and  $\Delta t$  with rising  $U_s$ . The experimental parameters are  $\lambda = 796.1 \text{ nm}$ ,  $N = 1.5 \times 10^6$ ,  $P_+ = 500 \text{ mW}$  and  $F = 87000$ . In the simulations atom number and pump power are fitted to  $1.9 N$  and  $0.6 P_+$  in order to reach good quantitative agreement with the measurements. Good qualitative agreement is also reached if the simulations are performed with the measured parameters.

The backscattering rate strongly depends on the wavelength of the pump laser, when it is resonant to an eigenfrequency of the cavity [32]. This phenomenon can be understood as interference of the waves backscattered from all three cavity mirrors. From the experimental point of view, the most interesting feature is that backscattering can be avoided by a proper choice of the resonant cavity mode. The mirror-induced probe light power varies between almost 0 and 0.6% of the pump power.

Backscattered light in the probe mode represents an artificial instability, which seeds the collective dynamics. Consequently, increased mirror backscattering reduces the time delay  $\Delta t$ . On the other hand, the maximum probe light power  $P_{-,1}$  decreases with  $\Delta t$ , because the finite switch-on time limits the pump light available at this stage. This behavior is verified by the measurements shown in Fig. 4. For these measurements we vary the mirror backscattering by choosing different longitudinal cavity modes [32].

In the simulations shown in same figure, the finite switch-on time is taken into account. The atom number and pump power are fitted in order to reach good agreement with the experimental data, but the general behavior can be reproduced without free parameters. For a hypothetic sudden switch-on, we would expect a much weaker dependence of  $P_{-,1}$  on mirror backscattering.

The observation that increased mirror backscattering leads to a faster rise of the collective dynamics only applies, when the amount of mirror backscattering is smaller than the atomic coupling strength  $U_s < NU_0$ , which is true for the above given values. For a reduced

atom number of about  $N \sim 10^5$  though, mirror backscattering is on the same order of magnitude as the atomic coupling. In this case, it is able to suppress the collective dynamics, which we do observe experimentally. When we use Bose-Einstein condensed clouds, atom numbers are precisely on the order of  $10^5$ . It is therefore necessary to resort to cavity modes with ultra-low mirror backscattering. To control and cancel the amount of mirror backscattering, we have developed a method described in [32] based on the injection of an additional light field into the probe mode of the cavity.

### C. Pump power

The dynamics of the collective instability depends on the pump light power. A reduction of pump power leads to a decrease of the contrast of the optical standing wave resulting from the interference of the pump and probe modes. This weakens the collective dynamics. In previ-

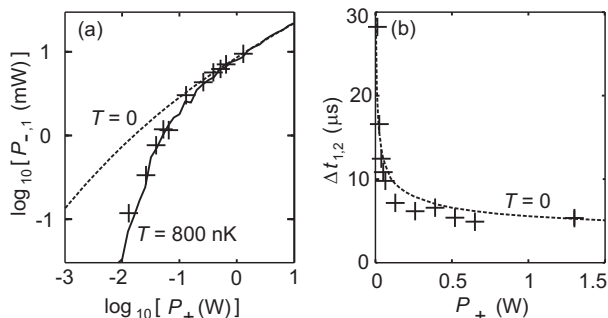


FIG. 5: Influence of the pump light power on (a) the peak probe power  $P_{-,1}$  and (b) the time delay between the first and the second superradiant peak  $\Delta t_{1,2}$ . Simulations are without free parameters. Residual fluctuations in the simulation for  $T = 800$  nK in (a) are due to a limited simulated atom number. Experimental parameters are  $\lambda = 796.1$  nm,  $N = 2.4 \times 10^6$ , and  $F = 87000$ . The stochastic error lies within the size of the markers.

ous experiments [8], where the CARL has been exposed to the dissipative and diffusive forces of an optical molasses, we observed a threshold behavior in the pump power. In contrast, the present setup lacks a strongly dissipative reservoir, so that it is unclear whether CARL with BECs can show a threshold behavior. The only channel available to dissipation in this setup is transmission through the cavity mirrors. This provides a coupling of the cavity modes to the electromagnetic field of the surroundings, which to good approximation can be regarded as a zero-temperature reservoir of photons. One therefore would expect dissipation without diffusion.

We observed that temperature effects can lead to a threshold-like behavior, if the atoms are not Bose-condensed. Fig. 5(a) shows measurements of the maximum probe light power  $P_{-,1}$  as a function of the pump power  $P_+$ . The data agree very well with simulations

(solid line) using the parameters specified in the captions of Fig. 5 and a temperature of the atoms of  $T = 800$  nK. The dotted line is a simulation with the same parameters, but at temperature  $T = 0$ . Down to a pump power of about  $P_+ \approx 0.1$  W, both curves coincide. Below this value the probe power is considerably reduced if the temperature of the atoms is finite. This demonstrates that thermal motion of the atoms can suppress the collective dynamics if the gain is not strong enough [34]. Another

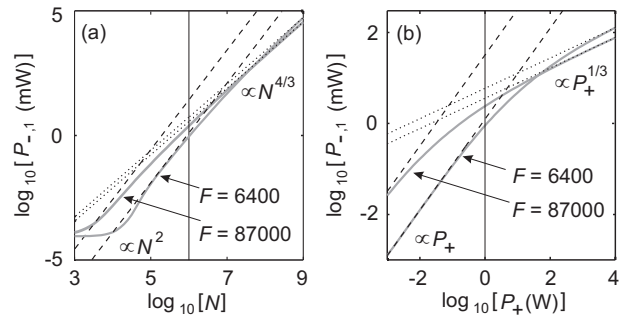


FIG. 6: Simulations (solid lines) of the transition from bad-cavity to good-cavity regime with respect to (a) atom number and (b) pump power. Each dependency is plotted for two values of the finesse  $F$ . The experimental parameters are  $P_+ = 1$  W in (a) and  $N = 10^6$  in (b). For the  $F = 87000$  simulations the wavelength is  $\lambda = 796.1$  nm for  $F = 6400$  it is  $\lambda = 795.3$  nm. The vertical lines in each figure show the value of the parameter held fixed in the other part of the figure. They characterize the region where our experiments take place. The dotted (dashed) lines show the asymptotic behavior typical for the good-cavity (bad-cavity) regime. The deviation of the simulations from the asymptotic behavior [solid curves in Fig. (a) below  $N = 10^4$ ] stems from mirror backscattering, which plays a major role for small atom numbers and suppresses the collective dynamics. The simulations are performed at  $T = 0$  in order to show the underlying physics without being influenced by temperature effects.

observable which depends on the pump power is the time difference  $\Delta t_{1,2}$  between the first and the second superradiant light pulse. This time difference corresponds to the typical time-scale, on which the atomic momentum distribution is shuffled between different momentum states. The stronger the pump power is, the faster the momentum distribution changes. This connection is shown in Fig. 5 (b), where the data agree very well with a simulation with the above given parameters and an atomic temperature of  $T = 0$ . A simulation with the realistic atomic temperature of  $T = 800$  nK hardly differs from the  $T = 0$  curve and is omitted in Fig. 5 (b) for clarity. This shows that the time difference  $\Delta t_{1,2}$  is quite insensitive to the momentum spread of the atoms.

### D. Finesse

The CARL model comprises different regimes, which are denoted as good-cavity and bad-cavity regime. While



former work in our group was performed in the good-cavity regime [8, 35], the SRyS experiments are very far in the bad-cavity regime [10, 24]. With our new apparatus we are able to reach both regimes by varying the finesse of the cavity and to find characteristic signatures of the regimes in the comportment on certain experimental parameters. The maximum probe light power scales in the good-cavity regime with  $P_{-,1} \propto N^{4/3} \cdot P_+^{1/3}$  and in the bad-cavity regime with  $P_{-,1} \propto N^2 \cdot P_+$  [5]. Which regime is reached does not only depend on the finesse  $F$ , but also on the atom number and the pump power themselves. As discussed in Sec. II C, the regime is determined

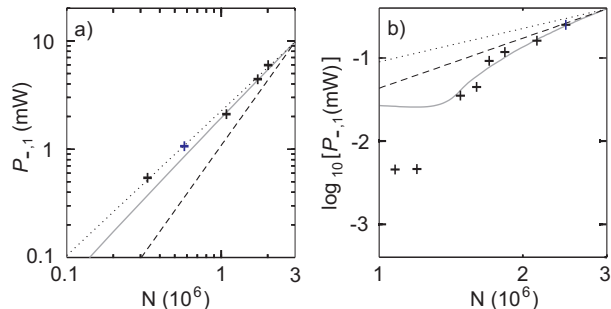


FIG. 7: Measured dependency of the maximum probe light power as a function of atom number for values of the finesse of (a)  $F = 87000$  and  $F = 6400$ . The parameters are a)  $\lambda = 796.1$  nm,  $P_+ = 1.43$  W and b)  $\lambda = 795.3$  nm,  $P_+ = 66$  mW. Comparing the data points to the asymptotic behavior shown in the dotted and dashed lines the situation in a) can be identified as good-cavity regime and the situation in (b) as bad-cavity regime. The behavior is confirmed by simulations with no free parameters (solid lines). The values of the data points are scaled by (a) 0.75 and (b) 2.8 in order to improve agreement with the simulation. This systematic error of the data points is due to uncertainties in the calibration of the probe light power. These depends on the polarisation of the light and for this reason we have to apply different scalings for low and good finesse. Nevertheless the dependency on atom number, which in the logarithmic plot shows up as a different slope is not changed by this pure multiplication. The stochastic error lies within the size of the markers.

by the relative size of the cavity decay rate,  $\kappa_c \sim F^{-1}$ , and the gain bandwidth which depends on the collective gain  $G \sim nNU_0^2/\kappa_c$ . Hence, the good-cavity regime is characterized by large atom numbers and large pump powers, and the bad-cavity regime by small atom numbers and small pump powers. This feature is shown in Fig. 6, where the dependence is simulated for the two values of the finesse accessible to our experiment. As can be seen, the transition between the two regimes is not sudden, but spreads across a wide range of atom number and pump power.

Measurements of the dependence of the maximum probe light power on atom number are shown in Fig. 7. The finesse of the ring cavity can be set to either  $F = 87000$  in Fig. (a) or  $F = 6400$  in Fig. (b) by simply rotating the polarization of the pump light with respect to the symmetry plane of the cavity. This enables us o

probe both, the good-cavity and the bad-cavity regime. The asymptotic dependency in the good-cavity regime is shown by dotted lines, the dependency in the bad-cavity regime by dashed lines. The solid line represents a simulation with no free parameters. By varying the atom number in (a) between  $N_1 = 3 \cdot 10^5$  and  $N_2 = 2 \cdot 10^6$  the corresponding CARL parameters [Eq. (7)] [5] are  $\rho_1 = 4.7$  and  $\rho_2 = 7.0$ , the corresponding scaled decay rates are  $\kappa_1 = \kappa_c/\omega_T\rho_1 = 0.3$  and  $\kappa_2 = 0.2$ . The conditions  $\kappa_{1,2} < 1$  and  $\rho_{1,2} > 1$  are typical for the semi-classical good-cavity regime. Indeed, the data points are lying close to the good-cavity theoretical lines. In Fig. 7(b) the measured atom numbers between  $N_3 = 1.1 \cdot 10^6$  and  $N_4 = 2.5 \cdot 10^6$  correspond to CARL parameters between  $\rho_3 = 5.1$  and  $\rho_4 = 6.7$  and scaled decay rates between  $\kappa_3 = 3.7$  and  $\kappa_4 = 2.8$ . The conditions  $\kappa_{3,4} > 1$  and  $\rho_{3,4} > \kappa_{3,4}$  are typical for the semi-classical bad-cavity regime. This is confirmed by the data points which seem to be approximated by the good-cavity asymptotic line for high atom numbers. The discrepancy for low atom numbers is due to mirror backscattering. This effect is also visible in the simulation.

## E. Temperature

With our apparatus the atomic temperature can be varied within a range from below one  $\mu\text{K}$  to several tens of  $\mu\text{K}$ . This allows us to systematically examine the in-

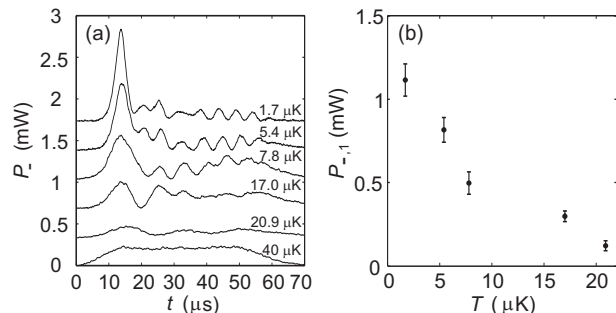


FIG. 8: (a) Measured time signal of the probe-light for different atomic temperatures. For clarity the curves are shifted by 0.35 mW from each other. The experimental parameters are for all curves  $N = 10^6$ ,  $\lambda = 796.1$  nm and  $F = 87000$ . The signal decreases and the contrast is washed out for rising temperature. (b) Maximum probe-light power as a function of temperature extracted from (a).

fluence of the temperature on the collective dynamics and identify the role of quantum statistics in the dynamics of CARL and SRyS. Fig. 8(a) presents recorded time signals of the probe light for different temperatures.

The curves show characteristic trains of superradiant pulses. With rising temperature the maximum probe-light power decreases and subsequent pulses are washed out. The bottom curve, which corresponds to a temperature of  $T = 40$   $\mu\text{K}$ , shows no modulation of the

light power and resembles the time evolution of pure mirror backscattering. The decrease of the maximum probe light power is separately plotted in (b). Obviously, a rising temperature leads to a suppression of the collective dynamics. This can be explained by the fact that the self-amplified optical standing wave has to arrange the atoms into an atomic grating. This is only possible if the depth of the optical lattice is larger than the thermal energy of the atoms. For that reason a rising temperature leads to fewer atoms participating in the gain mechanism. This is the reason why we cannot see CARL activity in the present experiment with atom numbers of  $N = 10^6$  at a temperature of  $T = 40 \mu\text{K}$ , while we observed CARL in recent experiments with atom numbers of  $N = 10^7$  at temperatures well above  $T = 100 \mu\text{K}$  [7, 8]. The fact that CARL is observable at all with thermal clouds of atoms, is the proof that quantum statistical phenomena do not play a role for the dynamics of CARL.

### F. Evaluation of absorption images

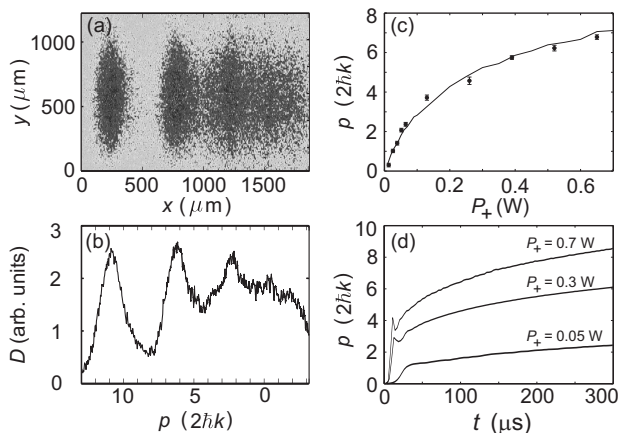


FIG. 9: (a) Typical absorption image of a thermal atomic cloud after the CARL dynamics and 10 ms ballistic expansion. (b) Vertically integrated optical density of the cloud. (c) Measured mean momentum as a function of pump power compared to a simulation with no free parameter. (d) Simulated time evolution of the mean momentum. The momentum is given in units of the recoil momentum  $p_r = 2\hbar k$ . The experimental parameters are  $\lambda = 796.1 \text{ nm}$ ,  $N = 2.4 \times 10^6$  and  $F = 87000$ . The atomic temperature is  $T \simeq 1 \mu\text{K}$ .

After a time period where the atoms are exposed to collective dynamics, the atoms are released from the magnetic trap. The atomic cloud expands ballistically, and after a time-of-flight of typically  $t_{\text{TOF}} = 10 \text{ ms}$  an absorption image is recorded, revealing the momentum distribution of the atoms in the trap. Fig. 9(a) shows a typical image of a thermal atomic cloud with (b) the vertically integrated optical density. The momentum can be calculated from the horizontal displacement of the atoms. Individual momentum states cannot be resolved, because the momentum distribution appears broadened

by the thermal motion. Nevertheless, interesting information like the mean momentum  $\langle p \rangle$  can be extracted from such images. Therefore, we calculate the center-of-mass of the vertically integrated optical density. This mean momentum can be examined as a function of the experimental parameters. Fig. 9(c) shows this dependency of the pump power. The measurements are very well reproduced by simulations of the CARL equations. The simulations in Fig. 9(d) show that the mean momentum increases rapidly during the first  $T = 50 \mu\text{s}$  and then starts to saturate. The saturation is due to the presence of the optical cavity restricting the range of accessible momentum states. In the simulations, we assume a realistic temperature of  $T = 1.2 \mu\text{K}$ . The strong spatial modulation of the atomic density in Fig. 9(a) depicts the momentum distribution generated by the collective dynamics. This behavior is qualitatively supported by simulations.

If as shown in Fig. 10 a Bose-Einstein condensate is used, we are able to resolve individual momentum states for (a) no pump light-field and (b) a pump light-power of  $P_+^{\text{max}} \approx 1 \text{ W}$ . Due to the short interaction time of the BEC with the light-field of  $t_{\text{ia}} \approx 40 \mu\text{s}$  only two superradiant maxima are observed in (c). The measured atomic momentum distribution after the interaction in (d) shows a depopulation of the  $|p\rangle = |0\rangle$  state and a shift towards momentum states with positive momentum. The substantial population of the momentum state with negative momentum  $|p\rangle = |-1\rangle$  is due to the semiclassical behavior of the system and is equivalent to the observation of momentum spread in [24].

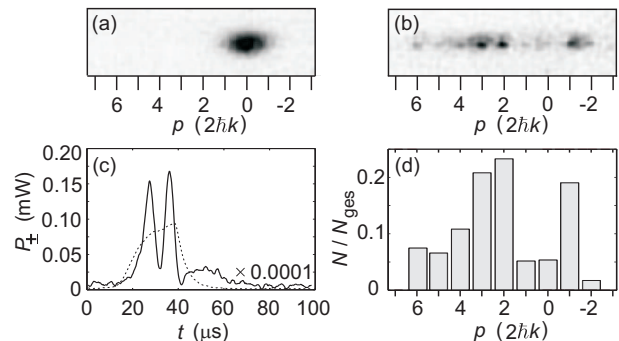


FIG. 10: Absorption images of Bose-Einstein condensates after 10 ms ballistic expansion (a) without CARL and (b) with CARL activity. (c) Simultaneously recorded pump (dashed line) and probe power (solid line). Pump power is scaled down by  $10^{-4}$ . (d) Momentum distribution derived from Figure (b).

## IV. CONCLUSION

We conclude this paper with the statement, that the collective atomic recoil laser and superradiant Rayleigh scattering are two faces of the same medal. Previous

theoretical work [36] has shown that the characteristic quantity distinguishing both effects is the collective gain bandwidth compared to the cavity decay rate. Our experiment is designed to give access to both regimes, the superradiant (or bad-cavity) regime and the good-cavity regime. The observed characteristic dependence of the instability amplitude on the atom number allows us to clearly identify the regimes, and to experimentally demonstrate the intrinsic link between both phenomena.

Another important result is the presence of collective instabilities at high temperatures. In earlier experiments, CARL dynamics have been observed with atomic clouds as hot as several 100  $\mu\text{K}$  [7]. This proves that the gain process underlying both, SRyS and CARL, is not based on quantum statistics, but on cooperativity [16]. From this results a better understanding of the intricate relationship between CARL and superradiance.

This experiment represents the first study of Bose-Einstein condensates in macroscopic cavities. For the experiments described within this publication though, the quantum degeneracy of the atoms is unimportant. However in future experiments, we want to study the role

of quantum statistics in a regime, where photonic and matter-wave modes are coherently coupled [37]. In this new regime the CARL dynamics may generate entangled states between atoms and scattered photons [27, 38].

Another challenge would be to reach the so-called quantum limit. This limit is distinguished from the semiclassical limit by the fact that the gain bandwidth is so small,  $\Delta\omega_G \gg \omega_r$ , that only adjacent momentum states of the atomic motion are coupled. This case (provided the temperature is very low) results in a train of self-similar superradiant pulses [20]. In our experiment this regime could be reached by enhancing the finesse of the ring cavity or by reducing  $\omega_r$ , e.g. by tuning the pump laser to an atomic resonance at a much higher frequency. To treat this regime the use of quantized atomic motion in the CARL equations is compulsory [20].

This work has been supported by the Deutsche Forschungsgemeinschaft (DFG) under Contract No. Co 229/3-1. We like to thank W. Ketterle for helpful discussions.

- 
- [1] R. H. Dicke, Phys. Rev. **93**, 99 (1954)
- [2] N. Skribanowitz, I. P. Hermann, J. C. MacGillivray, and M. S. Feld, Phys. Rev. Lett. **30**, 309 (1973).
- [3] R. L. Mößbauer, Z. Physik **151**, 124 (1958).
- [4] A. Steane, Appl. Phys. B **64**, 623 (1997).
- [5] R. Bonifacio and L. De Salvo, Nucl. Instrum. Methods **341**, 360 (1994).
- [6] R. Bonifacio and L. De Salvo, Appl. Phys. B **60**, S233 (1995).
- [7] D. Kruse, Ch. von Cube, C. Zimmermann, and Ph. W. Courteille, Phys. Rev. Lett. **91**, 183601 (2003).
- [8] C. von Cube, *et al.*, Phys. Rev. Lett. **93**, 083601 (2004).
- [9] S. Slama, S. Bux, G. Krenz, C. Zimmermann, and Ph. W. Courteille, Phys. Rev. Lett. **98**, 053603 (2007).
- [10] S. Inouye, *et al.*, Science **285**, 571 (1999).
- [11] M. Kozuma, *et al.*, Science **286**, 2309 (1999).
- [12] L. Fallani, *et al.*, Phys. Rev. A **71**, 033612 (2005).
- [13] A. T. Black, H. W. Chan, and V. Vuletić, Phys. Rev. Lett. **91**, 203001 (2003).
- [14] Th. Elsässer, B. Nagorny, and A. Hemmerich, Phys. Rev. A **69**, 033403 (2003).
- [15] G. Labeyrie, F. Michaud, and R. Kaiser, Phys. Rev. Lett. **96**, 023003 (2006).
- [16] M. G. Moore and P. Meystre, Phys. Rev. Lett. **86**, 4199 (2001).
- [17] W. Ketterle and S. Inouye, Phys. Rev. Lett. **86**, 4203 (2001).
- [18] Y. Yoshikawa, Y. Torii and T. Kuga, Phys. Rev. Lett. **94**, 083602 (2005).
- [19] N. Piovella, R. Bonifacio, B. W. J. McNeil, and G. R. M. Robb, Opt. Commun. **187**, 165 (1997).
- [20] N. Piovella, M. Gatelli, and R. Bonifacio, Opt. Commun. **194**, 167 (2001).
- [21] G. R. M. Robb, N. Piovella, and R. Bonifacio, J. Opt. B: Quantum Semiclass. Opt. **7**, 93 (2005).
- [22] M. Gangl and H. Ritsch, Phys. Rev. A **61**, 043405 (2000).
- [23] C. von Cube, *et al.*, Fortschr. Phys. **54**, 726 (2006).
- [24] D. Schneble, *et al.*, Science **300**, 475 (2003).
- [25] D. M. Stamper-Kurn and W. Ketterle, Proc. Les Houches Summer School, Session LXXII.
- [26] M. G. Moore, O. Zobay, and P. Meystre, Phys. Rev. A **60**, 1491 (1999).
- [27] N. Piovella, M. Cola, and R. Bonifacio, Phys. Rev. A **67**, 013817 (2003).
- [28] R. Bonifacio, L. De Salvo, and G. R. M. Robb, Opt. Comm. **137**, 276 (1997).
- [29] O. Zobay and G. M. Nikolopoulos, Phys. Rev. A **73**, 013620 (2006).
- [30] S. Slama, Ph.D. thesis, Universität Tübingen, 2007 (<http://www.uni-tuebingen.de/ub/elib/tobias.htm>).
- [31] M. Perrin, Zongxiong Ye, and L. M. Narducci, Phys. Rev. A **66**, 043809 (2002).
- [32] G. Krenz, S. Bux, S. Slama, and Ph. C. Courteille, Appl. Phys. B in press (2007).
- [33] C. Silber, *et al.*, Phys. Rev. Lett. **95**, 170408 (2005).
- [34] An interesting question in this context is, whether quantum fluctuations in a BEC could lead to stochastic and therefore diffusive processes, which then would cause a threshold behavior at zero temperature.
- [35] D. Kruse, *et al.*, Phys. Rev. A **67**, 051802(R) (2003).
- [36] R. Bonifacio, G. R. M. Robb, and B. W. J. McNeil, Phys. Rev. A **56**, 912 (1997).
- [37] P. Horak, S. M. Barnett, and H. Ritsch, Phys. Rev. A **61**, 033609 (2000).
- [38] M. G. Moore and P. Meystre, Phys. Rev. A **59**, R1754 (1999).